Soils and Rocks
www.soilsandrocks.com
An International Journal of Geotechnical and Geoenvironmental Engineering
ISSN 1980-9743
ISSN-e 2675-5475

The influence of the fluid dielectric constant on the shear strength of a unsaturated soil

M.S.S. Almeida[1,#], S.L. Machado[2], H.M.C. Andrade[2]

Article

Keywords
Dielectric constant
Napl
Shear strength
Unsaturated soils

Abstract
Results of triaxial tests performed in saturated and unsaturated compacted soil specimens with different interstitial fluids are presented. Tests were carried out in order to study the influence of the fluid relative dielectric constant, ε_r, on the soil shear strength of a granite-gneiss clayey residual soil from Salvador, Bahia, Brazil. It is shown that the soil shear strength is affected not only by the interstitial fluid saturation degree (or suction) but it is also a nonlinear function of the interstitial fluid value of ε_r. The shear strength of the saturated samples decreased with ε_r, following the order (air $\varepsilon_r = 1$, diesel $\varepsilon_r = 2.13$, ethanol $\varepsilon_r = 24.3$ and water $\varepsilon_r = 80$), whereas fluids with higher dielectric constants presented a more pronounced increase in shear strength under drying (replacement of the interstitial liquid with air). An empirical model is proposed to predict soil shear strength as a function of $(\varepsilon_{rw} - \varepsilon_f)$, the difference between the relative dielectric constant of the water and the interstitial fluid. Good adherence between experimental and fitted results was obtained.

1. Introduction

According to Garcia et al. (2004), leaks of organic and inorganic products that occur in fuel tanks and pipes are the most common cause of contaminant releases to the environment. Besides the possible contamination, the presence of these substances can affect the soil stress-strain behavior depending on the soil-fluid interaction, which differs according to the physical-chemical properties of the fluids involved. It can be said, however, that studies concerning the mechanical behavior of soil when saturated by different interstitial fluids, such as hydrocarbons, are still scarce. Almost all the papers published since the 1980s (Brown & Anderson, 1983; Brown & Thomas, 1984; Brown & Thomas, 1986; Fernandez & Quigley, 1985; Schramm et al., 1986; Budhu et al., 1991; Li et al., 1996; Oliveira, 2001) focus on the hydraulic behavior of the soil when percolated by different fluids.

The fluid polarity can be evaluated by its dielectric constant. The value of ε_r can be calculated by the ratio between the charge storage capacity of a capacitor filled with the medium of interest with that of the same capacitor with vacuum between the plates. According to Halliday et al. (2007), ε_r is related to the ability of the fluid molecules to polarize, orienting their poles under an electric field. For three phase media such as the soil, the value of ε_r can be estimated through semi-empiric formulas such as the CRIM (Complex Refractive Index Method, comprised by Equation 1), which relates the dielectric constant of a unsaturated porous medium with its porosity, *n*, and the water degree of saturation, *Sr*. Although this equation was originally proposed for water, its use can be extended for a unsaturated porous medium partially filled with other interstitial fluids.

$$\sqrt{\varepsilon_r} = n \cdot Sr\sqrt{\varepsilon_{rw}} + (1-n)\sqrt{\varepsilon_{rs}} + n(1-Sr)\sqrt{\varepsilon_{rair}} \quad (1)$$

where ε_r, ε_{rw}, ε_{rs} e ε_{rair} are, respectively, the relative dielectric constant of the soil as a whole, water, solid particles and air. Table 1 shows ε_r typical values for different materials (Davis & Annan, 1989). Most minerals have ε_r values between 4 and 5. These values are near to the minimum values presented in Table 1 for silt, sand, and clay.

Anandarajah & Zhao (2000) evaluated the shear strength of a clay when saturated by fluids of different dielectric constants. The samples were saturated and tested in a triaxial equipment. The fluids used in the tests were formaldehyde ($\varepsilon_r = 111$), water ($\varepsilon_r = 80$), ethanol ($\varepsilon_r = 24.3$), acetic acid ($\varepsilon_r = 6.16$), triethylamine ($\varepsilon_r = 2.42$) and heptane

[#]Corresponding author. E-mail address: mario_almeida10@yahoo.com.br.
[1]Universidade Federal do Recôncavo da Bahia, Cruz das Almas, BA, Brazil.
[2]Universidade Federal da Bahia, Salvador, BA, Brazil.

Submitted on December 14, 2018; Final Acceptance on June 10, 2020; Discussion open until March 31, 2021.
DOI: https://doi.org/10.28927/SR.434535

Table 1. Typical values of the relative dielectric constants for different materials.

Material	Relative dielectric constant (ε_r)
Air	1
Water	80
Diesel	2.13
Ethanol	24.3
Solid particles	4-5
Dry sand	3-5
Silt	5-30
Clay	5-40

Source: Adapted from Davis & Annan (1989).

(ε_r = 1.91). Figure 1 presents the results obtained by the cited authors. As can be noted, the soil shear strength varies non-linearly with ε_r.

Di Maio et al. (2004) studied the shear strength of two clays from Italy (Bisaccia clay and bentonite Ponza) when saturated with water, NaCl solutions and cyclohexane. According to these authors, the minimum values of shear strength for both clays occurred when the specimens were saturated with water. The use of interstitial fluids with ε_r values lower than water increased soil shear strength. Calvello et al. (2005) found similar results when performing direct shear and unconfined compression tests in soil samples saturated with distillate water, salt solutions in different concentrations and organic fluids with different dielectric constants.

The influence of the interstitial fluid polarity on the soil shear strength values is explained, at least partially, by the double layer theory. The most widely accepted conceptual model to represent the interactions between the fluid and the clay surface is the diffuse double layer system. This model is an evolution of the Helmholtz-Smoluchowski theory proposed by Helmholtz (1879-1914; see Helmholtz, 1879) and improved by the work of Gouy-Chapman (1910-1913). The diffuse double layer system consists of the clay particles, adsorbed cations, and water molecules in one layer, while the other layer is a diffuse swarm of counterions. Although this model does not take into account the effect of the potential energy in the oriented molecules of water that surround the clay particles, it is useful to explain some basic phenomena in a clay-water-electrolyte system (Fang, 1997).

Equation 2 can be used to predict the double layer thickness, *t*, based on the Gouy-Chapman theory (Gouy, 1910). It can be seen from Equation 2 that an increase in the electrolyte concentration or a decrease in the fluid dielectric constant reduces the double layer thickness, bringing the particles closer to each other and increasing soil particle interaction forces.

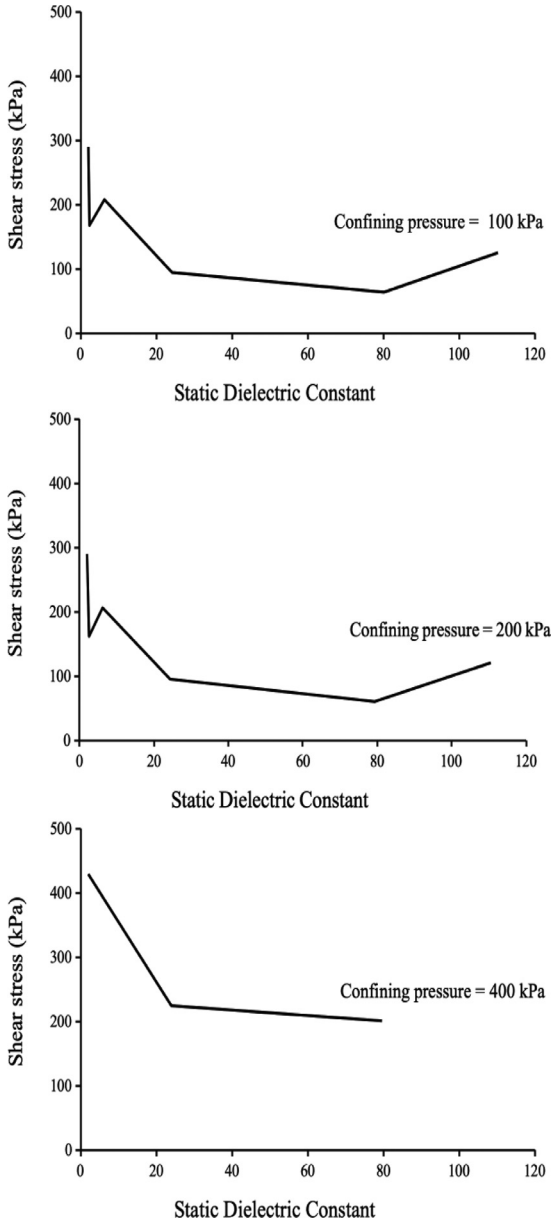

Figure 1. Shear strength variation with ε_r. Source: Adapted from Anandarajah & Zhao (2000).

$$t = \sqrt{\frac{\varepsilon . k_b T}{8\pi n_e e^2 v^2}} \quad (2)$$

In Equation 2, ε is the dielectric constant, K_b is the Boltzmann constant, T is the temperature, n_e is the electrolyte concentration, e is the elementary charge and ν is the ionic valence. In this paper, an investigation is performed about how the shear strength of a residual soil of granite-gneiss is affected when its voids are filled, in different proportions, with fluids of dielectric constants smaller than water.

2. Testing materials and methods

2.1 Materials - soil

The soil used in this study was a granite-gneiss residual soil, RGG, which is predominant in the city of Salvador, BA, Brazil. The geotechnical characterization tests were executed according to the following standards: NBR 7181 (ABNT, 1984); NBR 6489 (ABNT, 1984); NBR 7180 (ABNT, 1984); NBR 6508 (ABNT, 1984) and NBR 7182 (ABNT, 1986). Table 2 presents the main RGG geotechnical characteristics (void ratio, *e*, and porosity, *n*, correspond to optimum compaction conditions, normal Proctor energy).

Complementary tests were also performed on RGG specimens in order to determine specific surface area, SS, pore volume, PV, chemical composition and liquid retention curves, SLRC, besides optical microscopy analysis. SS and PV were determined using the physisorption of N_2 technique, B.E.T. method (Brunnauer et al., 1938) and a Micromeritics ASAP 2020 Porosimetry System. Samples were heated at 300 °C for 12 h in vacuum (≈267 Pa) for the removal of water or any other physisorbed substances prior to the tests.

The effects of soil texture on the values of the SS values were analyzed by preparing the samples in four different conditions: a) material passing through the sieve #10 and retained on the sieve #16; b) material passing through the sieve #80; c) material passing through the sieve #200; and d) clay fraction obtained in a sedimentation procedure. Specimen mass for each test was about 0.20 g. Table 3 presents the obtained results. More results are available in Almeida (2016). The SS values of the clay fraction, according to Hillel (1980), indicate the presence of the minerals kaolinite and ilite.

Optical microscopy was performed according to procedures proposed by Kaya & Fang (2005). A 10 mL beaker was filled with a solution containing 10 % of the soil and 90 % of the given fluid (water, ethanol, or diesel) in weight and then stirred for one minute in order to improve soil-fluid interactions. After that, a drop of the solution was poured onto a glass streak plate and then taken to the optical microscope (Olympus brand, BX41 model, 100x resolution and attached photographic camera Olympus brand, Evolt E330 model). Figure 2 presents the results of the optical microscopy analyses. In this figure it is possible to visualize the effect of each fluid in terms of soil flocculation/dispersion (tests were performed in duplicate). Samples with high polarity interstitial fluid (water) tended to present a disperse structure, whereas samples immersed in diesel presented a flocculated structure. Ethanol (intermediate ε_r) presented an intermediate behavior.

Table 3. RGG specific surface and pore volume in different texture conditions.

Material	SS (m^2/g)	PV (cm^3/g)
Passing through the sieve #10 and retained on the sieve #16	44.2	0.197
Passing through the sieve #80	50.8	0.240
Passing through the sieve #200	72.0	0.342
Clay	83.7	0.420

RGG elementary composition was determined using the X-ray fluorescence technique (EDX) and an EDX-720 Shimadzu spectrometer. RGG powder samples were analyzed in 5mm polypropylene holders, tightly covered with a 5 μm polypropylene film. The X-rays fluorescence spectra were collected in a vacuumed environment. Tests were performed in a single batch of sixteen samples retrieved from a

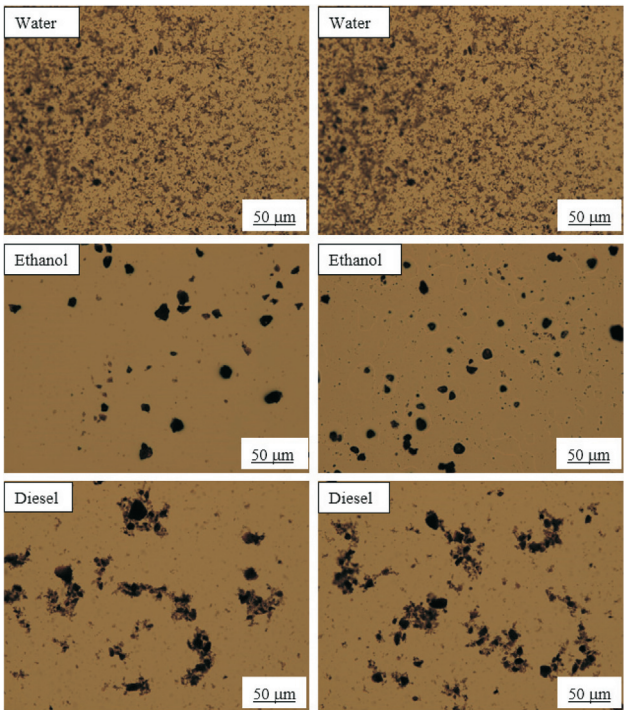

Figure 2. Optical microscopy images of RGG samples immersed in different fluids.

Table 2. Results from the geotechnical characterization of the residual granite-gneiss soil.

Grain size composition (%)			Atteberg limits (%)			Compaction normal Proctor energy		γ_s (kN/ m^3)	*e*	*n*
Sand	Silt	Clay	W_L	W_P	I_P	γ_{dmax} (kN/m^3)	w_{ot} (%)	27.04	1.03	0.51
26	18	56	78	42	36	13.34	31.80			

compacted specimen (four samples at the top, four at the bottom and eight samples at the middle portion of the specimen). Table 4 summarizes the obtained results from EDX tests. It can be observed that silicon, aluminum, and iron are the main oxides found in the RGG specimens, comprising 98.86 % ± 0.09 of all detected oxides. TiO_2, BaO, SO_3, MnO and ZrO_2 are the main remaining oxides in the samples (1.14 % ± 0.13). The SiO_2/Al_2O_3 ratio was about 1.15, indicating the predominance of the kaolinite mineral group (1:1 structure).

2.2 Materials - fluids

Water, diesel, and ethanol were the interstitial fluids used in this study. Their density, viscosity and superficial tension were determined in the laboratory. A Krüs Easydyne Tensiometer, k20 model, was used for superficial tension determination. Temperature was controlled using a Brookfield bath, TC-550 model. Fluids were tested at 15, 20, 25, 30, 35 and 40 °C. Once the temperature of equilibrium was reached, the densities of the fluids were determined using a standard volume of known density which was immersed in the fluid sample. After that, fluid superficial tension was determined using the ring method (ASTM D 971, 2012). A Brookfield viscometer, DV2T model, was used for the viscosity tests, which were performed at the same temperatures cited above (ASTM D 4016, 2014). Table 5 summarizes the obtained results for density, viscosity, and superficial tension of the fluids at 20 °C. More results are available in Almeida (2016).

2.3 Materials - soil-fluid interactions

Soil liquid retention curves, were determined in order to evaluate soil/fluid interactions. Compacted soil specimens (normal Proctor energy) at the optimum water content were used. The following techniques were used for suction control/measurement: direct suction measurement with tensiometers (water), adapted pressure plate (water, diesel), Richard's pressure chamber (water, diesel and ethanol) and filter paper (water). Tests were performed according to ASTM D 6836 (ASTM, 2008) and ASTM C 5298 (ASTM, 1994) when applicable. Figure 3 summarizes the results.

Experimental results were fitted by Equation 3, proposed by Fredlund & Xing (1994). For the sake of comparison, some results obtained for ethanol are also shown in Figure 3(b). As can be observed, the obtained results are close to those obtained for diesel. However, no suction-controlled tests were performed using ethanol.

The main water wetting branch was obtained by completely drying the sample from the optimum water content prior to the test. In the case of the main drying water branch, samples were first saturated from the optimum water content. The tests performed with diesel and ethanol, however, required that samples were first dried, then saturated with the fluid of interest, and finally left to dry by suction imposition. Because completely drying the samples induces non recoverable reduction in their void ratios, the experimental results are not completely comparable. Table 6 presents the main fitting parameters of the experimental results by Equation 3.

$$\theta = \theta_{sat}\left[1-\frac{\ln\left(1+\frac{\psi}{\psi_r}\right)}{\ln\left(1+\frac{10^6}{\psi_r}\right)}\right]\left[\frac{1}{\ln\left(e+\left(\frac{\psi}{a}\right)^n\right)}\right]^m \quad (3)$$

Table 4. Soil chemical composition by EDX.

Values	Chemical substances			
	SiO_2 (%)	Al_2O_3 (%)	Fe_2O_3 (%)	Others (%)
Average	46.83	40.65	11.38	1.14
SD	0.85	0.74	0.45	0.13
COV (%)	1.82	1.82	3.98	11.52

Table 5. Fluid properties at 20 °C.

Fluid	Superficial tension (mN/m)	Viscosity (cP)	Density (g/cm^3)
Diesel	25.98	3.08	0.829
Ethanol	24.45	1.67	0.845
Water	70.75	0.87	0.998

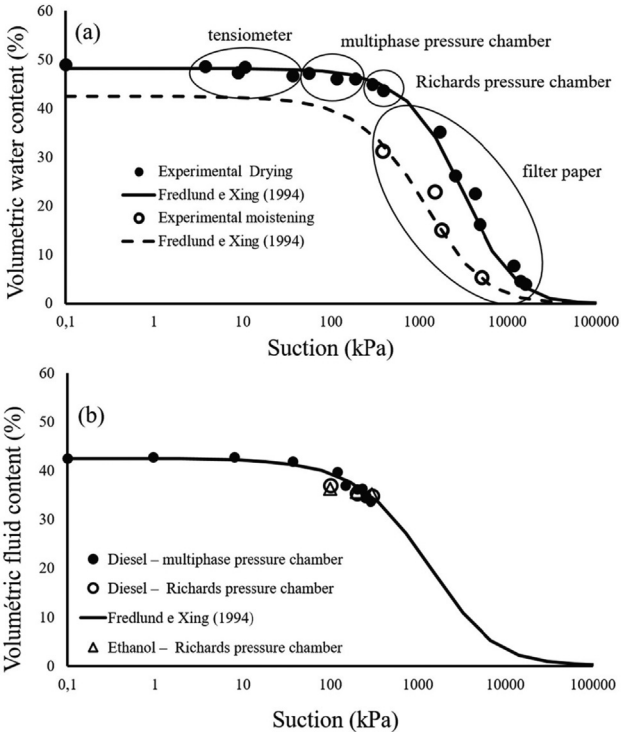

Figure 3. Retention curves for different fluids. Experimental data fitting using the Fredlund & Xing (1994) equation.

Table 6. Fitting parameters of experimental results by Equation 3.

Procedure	θ_{sat} (%)	θ_r (%)	ψ_r (kPa)	a	m	n	R^2
Main drying water	48.21	4.01	25 000	4929	3.98	1.20	0.99
Main wetting water	42.52	2.50	20 000	1818	3.80	1.05	0.90
Main drying diesel	42.51	2.50	20 000	2000	3.50	0.95	0.98

where θ is the volumetric content, θ_{sat} is the saturated volumetric content, ψ is the suction, ψ_r is the suction corresponding to residual volumetric content, e is the base of the natural logarithm, and a, n and m are fitting parameters.

3. Methods

3.1 Triaxial tests

Triaxial tests were performed on compacted samples (50 mm × 100 mm, nominal dimensions) in the same conditions as for SLRC tests. All tests were of the Consolidated Isotropically Drained type and performed in triplicate, by using different interstitial fluids (water, ethanol, diesel and dried soil, or air saturated). Tests were performed on saturated samples, with suction control or at a "constant" fluid content.

As all specimens were compacted at optimum water content in order to allow the use of different interstitial fluids, they were dried at atmospheric conditions (conditioned temperature room) for five days and then oven-dried at 70 °C for two days. Specimens were compacted in one single compaction batch. All the specimens were randomly chosen to be tested after compaction and drying procedures. Tests performed with saturated samples employed upward flow and back pressure saturation techniques ($B \geq 0.90$, where B is the Skempton's parameter). Specimens to be tested with suction control were first immersed after drying in the fluid of interest, water, ethanol or diesel, for at least 2 days and then taken to a Richard's chamber to impose the desired suction for at least 15 days. Finally, the specimens were transferred to a triaxial chamber (use of a porous stone with an high air entry value, HAEV, of 1,500 kPa in the chamber base) and the desired top, base and confining pressures were applied, adopting a net confining pressure of about $\sigma - u_a = 20$ kPa. Two more days were allowed for suction stabilization before triaxial tests began. Suction-controlled tests were performed (use of axis translation technique) employing suction values of 100 kPa, 200 kPa and 300 kPa. Air (top) and water (base) pressures were kept constant during all the tests.

In the case of the tests performed keeping a constant fluid content, the specimens were taken directly to the triaxial chamber after drying. The confining pressures adopted in the triaxial tests were 50 kPa, 100 kPa, 200 kPa and 400 kPa for tests with saturated/constant fluid content samples, and 50 kPa, 100 kPa, and 200 kPa for suction-controlled tests. Volume change readings of saturated specimens were performed employing the water pressure lines (top and base) and a volume change gauge. In the suction-controlled tests the fluid drainage of the specimens was performed by the triaxial chamber base and the volume change gauge was connected to the confining pressure line (externally made volume change measurements with chamber compressibility correction). The same procedure was used for the "constant" fluid content tests. In this case however, the top and base lines were open to the atmosphere to avoid excess pore water pressure generation. A PVC film with a small hole was used in the fluid exits to prevent evaporation. No fluid was observed being expelled from the specimens during the tests.

Axial Force and displacement measurements were performed externally to the triaxial chamber. Shearing rates were adopted taking into consideration the consolidation rate and the HAEV porous stone impedance in suction-controlled tests. All tests were performed by keeping the confining stress during the shearing phase constant. Tables 7 to 9 summarize the initial and final physical indexes

Table 7. Average physical indexes. Saturated samples.

Fluid	Confining stress (kPa)	Compaction				Saturated samples			
		γ_d (kN/m^3)	w (%)	CD (%)	n	After molding		After test	
					w (%)	n	w (%)	n	
Water	50	14.46	30.69	108.37	0.46	1.16	0.39	27.99	0.43
	100	14.31	30.43	107.27	0.47	1.24	0.39	27.17	0.42
	200	14.66	29.94	109.92	0.46	2.36	0.39	26.36	0.42
	400	14.64	30.29	109.77	0.46	1.72	0.39	26.45	0.42

Table 7 (cont.)

Fluid	Confining stress (kPa)	Compaction				Saturated samples			
		γ_d (kN/m^3)	w (%)	CD (%)	n	After molding		After test	
					w (%)	n	w (%)	n	
Ethanol	50	14.07	32.83	105.47	0.48	3.10	0.40	22.12	0.42
	100	14.04	32.66	104.94	0.48	2.73	0.41	22.50	0.42
	200	14.01	32.51	105.05	0.48	2.71	0.39	22.14	0.42
	400	14.09	32.18	105.62	0.48	3.87	0.41	22.24	0.42
Diesel	50	13.96	33.22	104.62	0.48	2.24	0.41	20.60	0.40
	100	13.98	33.52	104.82	0.48	4.27	0.41	20.18	0.40
	200	14.23	33.36	106.67	0.47	4.23	0.41	19.18	0.39
	400	14.12	33.20	105.82	0.48	4.01	0.42	20.17	0.40
Air	50	14.01	33.65	105.00	0.48	3.13	0.41	3.13	0.41
	100	14.00	32.66	104.97	0.48	2.38	0.41	2.38	0.41
	200	14.04	33.05	105.27	0.48	2.47	0.41	2.47	0.41
	400	14.08	32.33	105.57	0.48	1.91	0.40	1.91	0.40

Obs: CD is the compaction degree of the sample.

Table 8. Average physical indexes. Suction controlled samples.

Fluid	Suction (kPa)	Confining stress (kPa)	Compaction				After suction equalization		
			γ_d (kN/m^3)	w (%)	CD (%)	n	w (%)	n	Sr (%)
Water	100	50	14.43	30.68	108.17	0.47	29.80	0.46	94.58
		100	14.42	30.27	108.10	0.47	31.53	0.46	98.63
		200	14.32	30.26	107.37	0.47	30.62	0.47	95.30
Diesel	100	50	14.41	28.92	108.05	0.47	19.04	0.40	90.87
		100	14.50	29.37	108.67	0.46	19.30	0.40	92.57
		200	14.55	29.46	109.07	0.46	18.82	0.41	89.58
Water	200	50	14.51	29.31	108.77	0.46	29.33	0.45	95.84
		100	14.60	26.68	109.42	0.46	30.29	0.46	96.42
		200	14.35	30.74	107.57	0.47	29.57	0.46	95.42
Ethanol	200	50	14.53	30.63	108.90	0.46	18.96	0.41	86.25
		100	14.60	30.08	109.47	0.46	18.34	0.40	89.33
		200	14.60	30.42	109.42	0.46	18.96	0.40	89.10
Diesel	200	50	14.47	29.30	108.50	0.46	17.99	0.40	90.39
		100	14.50	29.41	108.67	0.46	17.79	0.40	87.17
		200	14.47	29.52	108.45	0.47	17.95	0.40	87.46
Water	300	50	14.21	31.06	106.52	0.47	28.92	0.47	90.69
		100	14.31	30.68	107.30	0.47	28.27	0.47	90.94
		200	14.25	30.85	106.82	0.47	29.56	0.47	90.66
Ethanol	300	50	14.32	31.27	107.37	0.47	18.59	0.40	88.57
		100	14.31	30.95	107.27	0.47	19.13	0.42	85.17

Table 8 (cont.)

Fluid	Suction (kPa)	Confining stress (kPa)	Compaction				After suction equalization		
			γ_d (kN/m^3)	*w* (%)	CD (%)	*n*	*w* (%)	*n*	*Sr* (%)
		200	14.38	30.27	107.77	0.47	18.39	0.41	82.52
Diesel	300	50	14.39	29.43	107.87	0.47	17.84	0.40	86.20
		100	14.31	29.95	107.27	0.47	17.38	0.40	83.96
		200	14.38	29.44	107.80	0.47	17.22	0.41	83.87

Obs: CD is the compaction degree of the sample.

Table 9. Average physical indexes. Constant water content.

Sr average (%)	Confining stress (kPa)	Compaction			Constant content samples after molding		
		γ_d (kN/m^3)	*w* (%)	CD (%)	*w* (%)	*n*	*Sr* (%)
14	50	14.42	30.69	108.10	3.49	0.40	14.16
	100	14.28	31.67	107.05	3.43	0.40	13.91
	200	14.76	30.80	110.64	3.49	0.40	14.16
	400	14.58	30.59	109.30	3.16	0.40	12.82
28	50	14.19	30.82	106.37	6.77	0.39	28.63
	100	14.30	31.59	107.20	6.58	0.39	27.83
	200	14.58	30.11	109.30	6.34	0.39	26.81
	400	14.52	31.07	108.85	6.52	0.39	27.58
42	50	14.58	28.86	109.30	9.32	0.38	41.12
	100	14.19	31.60	106.37	10.05	0.39	42.50
	200	14.08	30.76	105.55	10.21	0.39	43.18
	400	14.49	30.74	108.62	9.60	0.39	40.60
54	50	14.65	29.03	109.82	12.59	0.38	55.54
	100	14.43	30.66	108.17	12.96	0.39	54.81
	200	14.30	31.43	107.20	13.14	0.40	53.30
	400	14.53	31.08	108.92	12.74	0.39	53.88
66	50	14.52	30.55	108.85	15.86	0.41	61.71
	100	14.52	30.44	108.85	15.95	0.39	67.46
	200	14.29	31.13	107.12	16.50	0.39	69.78
	400	14.60	29.65	109.45	15.60	0.39	65.98
81	50	14.53	30.01	108.92	19.01	0.39	80.40
	100	14.67	29.84	109.97	18.64	0.39	78.83
	200	14.21	31.50	106.52	19.88	0.39	84.08
	400	14.41	30.93	108.02	19.39	0.39	82.01
87	50	14.55	29.92	109.07	22.16	0.41	86.23
	100	14.51	30.61	108.77	22.33	0.41	86.89
	200	14.40	31.11	107.95	22.76	0.41	88.56
94	50	14.50	30.46	108.70	25.53	0.42	95.33
	100	14.43	30.70	107.17	25.78	0.43	92.41
	200	14.33	31.38	107.42	26.18	0.43	93.84
	400	14.47	30.51	108.47	25.68	0.42	95.89

of the samples used in the triaxial tests. When applicable, tests followed the ASTM C 5298 (ASTM, 1994) standard.

4. Results and discussion

Figures 4 and 5 present typical stress/strain curves for the diesel and water saturated samples and suction controlled tests (ψ = 300 kPa) whereas Table 10 summarizes the obtained shear strength parameters for all the performed suction-controlled tests. The standard deviation of the experimental results around the fitted shear strength envelope, S_y and the coefficient of determination, R^2 are also shown. As can be observed, saturated diesel samples presented an over-consolidated behavior, reaching failure at low axial strains (2-4 %). Regarding the suction-controlled tests, this tendency is even more evident, with samples presenting brittle or fragile behavior.

Results presented in Table 10 were used to plot the graphs presented in Figures 6 and 7. Besides the expected shear strength envelope, the limits for the 95 % confidence interval (expected value ±1.96 S_y) are also presented in the figures. For the sake of comparison, Y axis scale was maintained the same for all the obtained results.

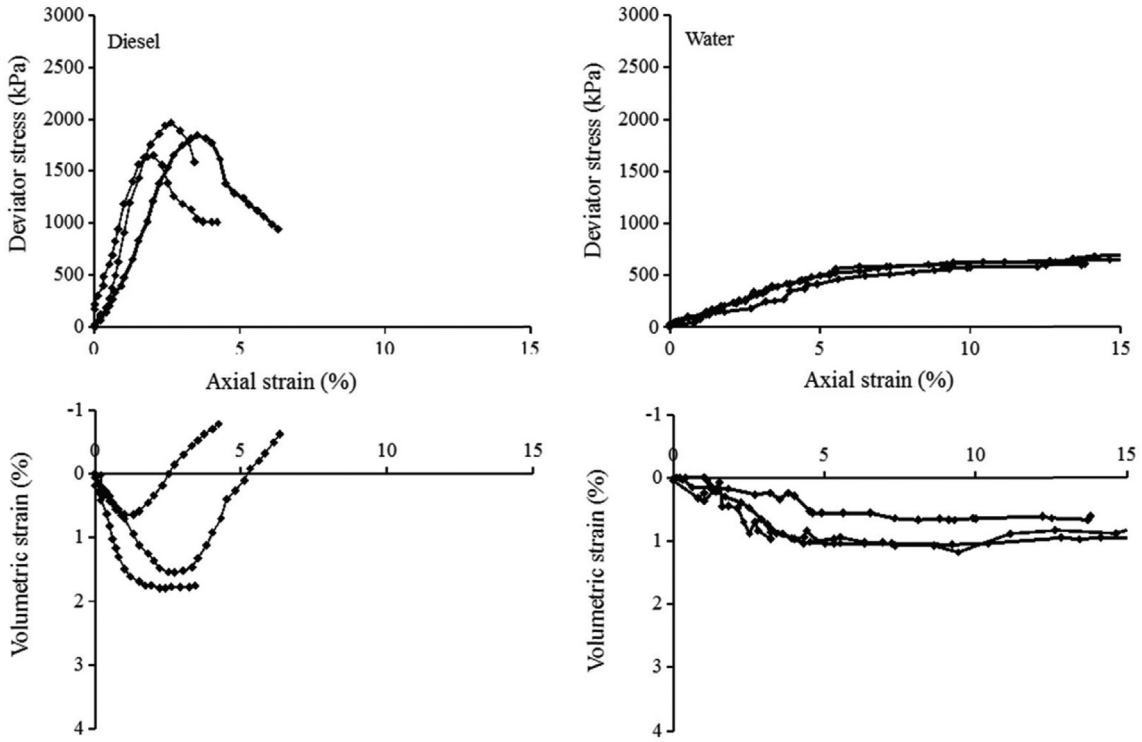

Figure 4. Stress/strain curves for saturated samples. σ_3 = 100 kPa.

Table 10. Shear strength parameters obtained in the tests.

Conditions	Fluid	ε_r	Suction (kPa)	c' (kPa)	ϕ' (graus)	S_y (kPa)	R^2
Saturated	Water	80.00	0	111.60	32.70	12.52	0.99
	Alcohol	24.3	0	137.40	39.60	21.67	0.99
	Diesel	2.13	0	344.30	39.00	51.54	0.95
	Air	1.00	0	466.20	48.50	34.53	0.99
Unsaturated	Water	74.65	100	133.10	14.10	8.61	0.85
		74.27	200	198.00	11.10	6.89	0.85
		67.41	300	286.60	8.90	6.81	0.83
	Diesel	2.01	100	159.70	54.20	36.81	0.98
		1.98	200	238.10	49.60	32.08	0.97
		1.93	300	169.50	53.80	46.23	0.96

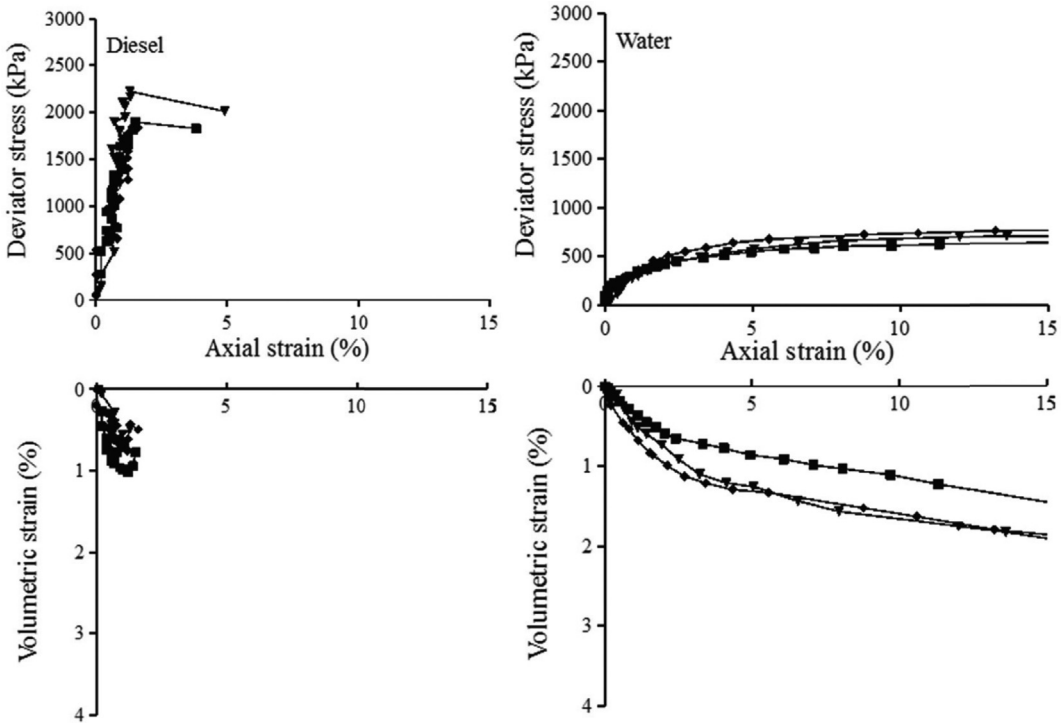

Figure 5. Stress/strain curves for suction controlled tests. ψ = 300 kPa and σ_3 = 100 kPa.

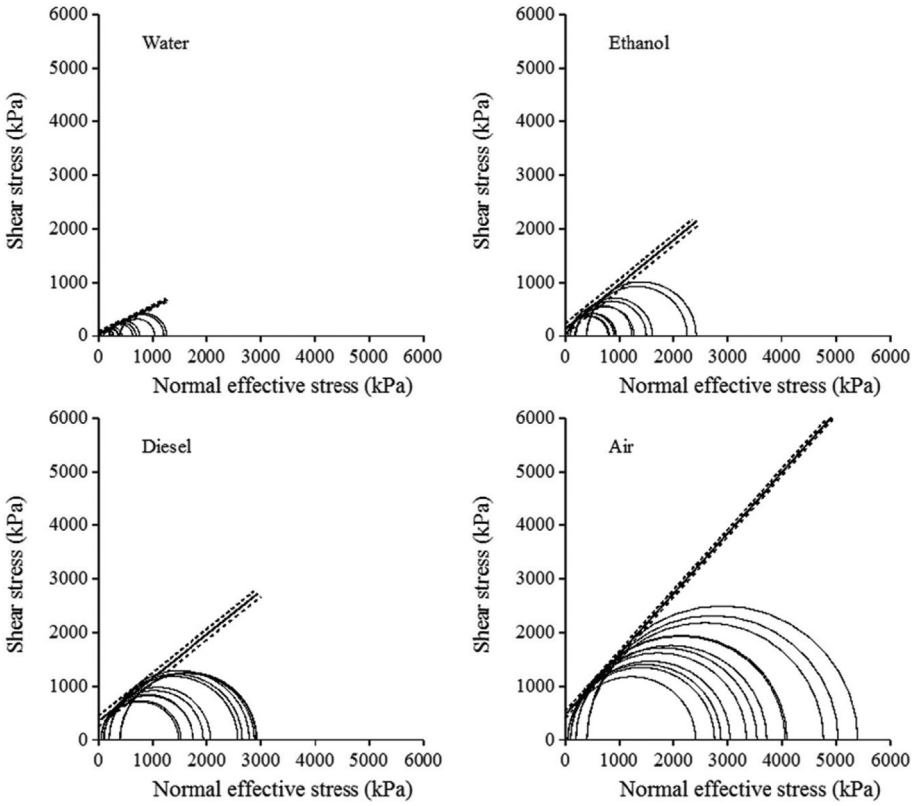

Figure 6. Shear strength envelopes for saturated samples.

It can be observed in Table 10 that in all the tests the shear strength decreases as the fluid polarity increases (air → diesel → alcohol and water, see Table 10). Figure 8 presents the shear strength values (deviator stress at failure,

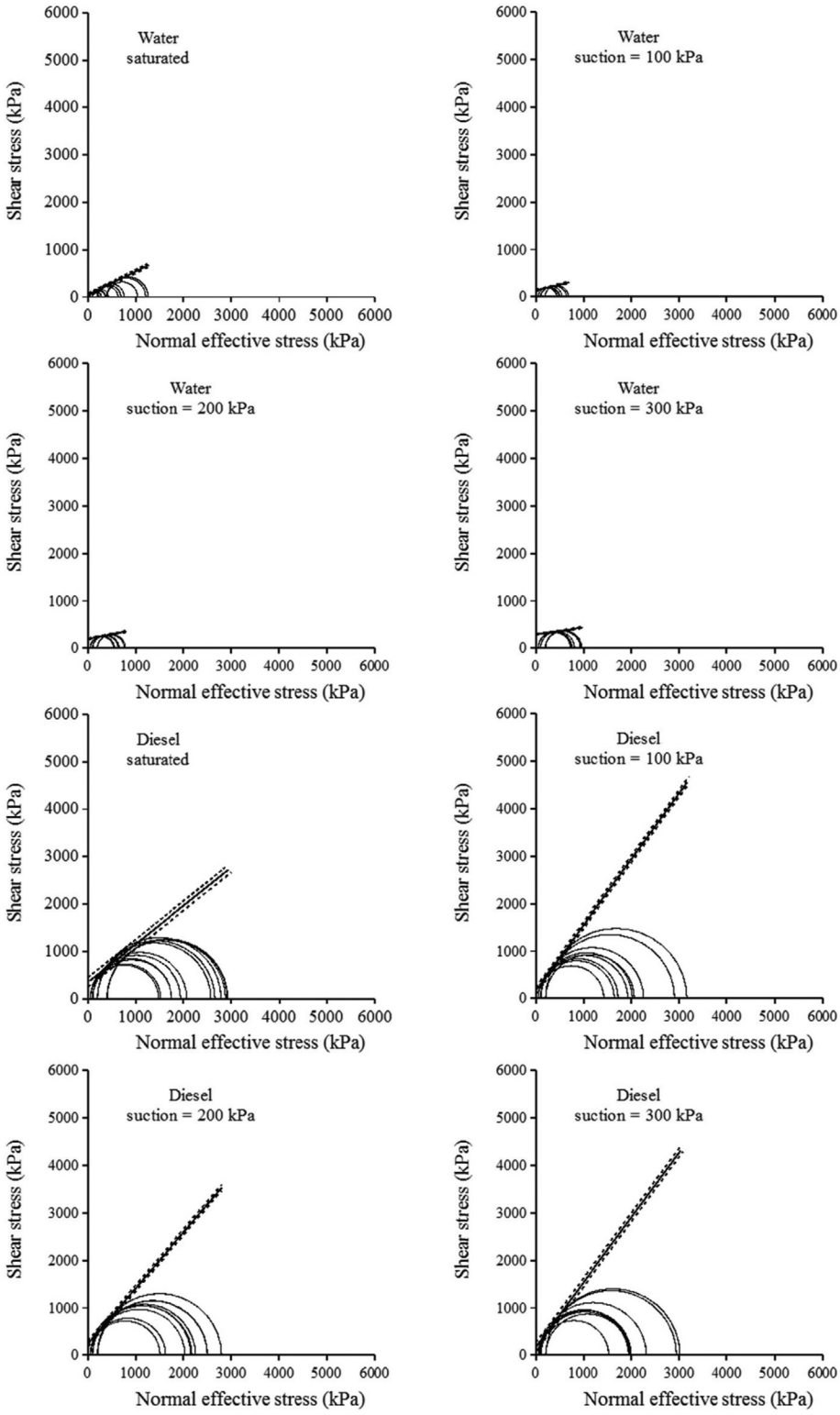

Figure 7. Shear strength envelopes for suction controlled tests.

q_{ff}) of the soil considering a confining stress of 200 kPa as a function of the fluid dielectric constant. For the case of unsaturated samples, the fluid dielectric constant was estimated through Equation 4.

$$\sqrt{\varepsilon_{rf}} = Sr\sqrt{\varepsilon_{rliq.}} + (1 - Sr)\sqrt{\varepsilon_{rair}} \quad (4)$$

where ε_{rf} - Relative dielectric constant of the interstitial fluid; S_r - Liquid degree of saturation; ε_{rliq} - Relative dielec-

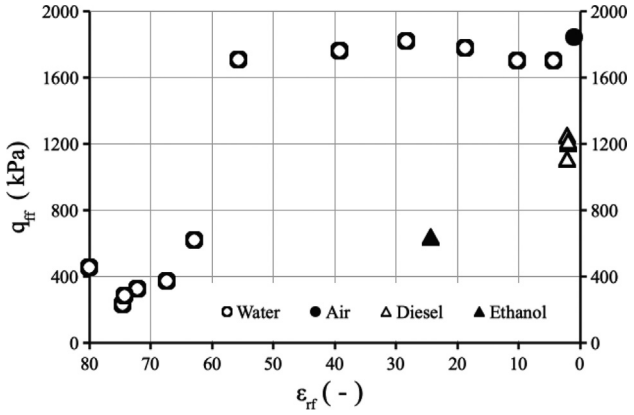

Figure 8. Shear strength values of the soil as a function of the fluid dielectric constant.

tric constant of the soil interstitial liquid (see Table 1); ε_{rair} - Relative dielectric constant of the air (~1).

It is evident that despite data scattering, q_{ff} decreases with an increase in ε_{rf}. Tables 11 to 13 summarize the obtained results for all the performed tests. As tests were performed in triplicate, the presented results are average values. Figure 9 presents the obtained results in terms of the ratio q_{ff}/q_{fw} vs. (ε_{rw} - ε_{rf}). The parameters q_{ff} and the q_{fw} correspond to the values of q at failure for tests performed with a fluid of interest (air, ethanol or diesel) and the fluid of reference (water). The paramters ε_{rliq} and ε_{rf} are the relative dielectric constants of the interstitial liquid and interstitial fluid (liquid + air) respectively. They are equal in saturated tests but differ in unsaturated ones. The parameter ε_{rw} is the

Table 11. Results and values adopted for the parameters of interest. Saturated samples.

Fluid	*Sr* (%)	σ'$_3$ (kPa)	q_{ff} (kPa)	q_{fw} (kPa)	q_{ff}/q_{fw}	ε_{rliq}	ε_{rf}	ε_{rw} - ε_{rf}	T_{sf} (10^{-3} N/m)
Air	0	50	1280.93	252.78	5.07	1.00	1.00	79.00	70.75
	0	100	1579.76	334.99	4.72	1.00	1.00	79.00	70.75
	0	200	1842.70	453.06	4.07	1.00	1.00	79.00	70.75
	0	400	2206.13	665.36	3.32	1.00	1.00	79.00	70.75
Diesel	100	50	734.27	252.78	2.90	2.13	2.13	77.87	25.98
	100	100	877.25	334.99	2.62	2.13	2.13	77.87	25.98
	100	200	1108.69	453.06	2.45	2.13	2.13	77.87	25.98
	100	400	1210.01	665.36	1.82	2.13	2.13	77.87	25.98
Ethanol	100	50	389.54	252.78	1.54	24.30	24.30	55.70	24.45
	100	100	470.73	334.99	1.41	24.30	24.30	55.70	24.45
	100	200	635.95	453.06	1.40	24.30	24.30	55.70	24.45
	100	400	971.00	665.36	1.46	24.30	24.30	55.70	24.45
Water	100	50	252.78	252.78	1.00	80.00	80.00	0.00	70.75
	100	100	334.99	334.99	1.00	80.00	80.00	0.00	70.75
	100	200	453.06	453.06	1.00	80.00	80.00	0.00	70.75
	100	400	665.36	665.36	1.00	80.00	80.00	0.00	70.75

Table 12. Results and values adopted for the parameters of interest. Suction controlled tests.

Fluid	*Sr* (%)	σ'$_3$ (kPa)	q_{ff} (kPa)	q_{fw} (kPa)	q_{ff}/q_{fw}	ε_{rliq}	ε_f	ε_{rw} - ε_{rf}	T_{sf} (10^{-3} N/m)
Water	96.17	50	192.74	107.25	1.80	80.00	74.65	5.35	70.75
	96.17	100	201.95	144.92	1.39	80.00	74.65	5.35	70.75
	96.17	200	232.42	247.44	0.98	80.00	74.65	5.35	70.75
	95.89	50	248.36	107.25	2.32	80.00	74.27	5.73	70.75
	95.89	100	269.99	144.92	1.86	80.00	74.27	5.73	70.75
	95.89	200	285.66	247.44	1.15	80.00	74.27	5.73	70.75
	90.76	50	344.36	107.25	3.21	80.00	67.41	12.59	70.75
	90.76	100	354.48	144.92	2.34	80.00	67.41	12.59	70.75

Table 12 (cont.)

Fluid	*Sr* (%)	σ'$_3$ (kPa)	q_{ff} (kPa)	q_{fw} (kPa)	q_{ff}/q_{fw}	ε_{rliq}	ε_f	ε_{rw} - ε_{rf}	T_{sf} (10^{-3} N/m)
	90.76	200	370.78	247.44	1.50	80.00	67.41	12.59	70.75
Diesel	91.01	50	776.18	252.78	3.07	2.13	2.01	77.99	25.98
	91.01	100	984.79	334.99	2.94	2.13	2.01	77.99	25.98
	91.01	200	1251.81	453.06	2.76	2.13	2.01	77.99	25.98
	88.34	50	852.85	252.78	3.38	2.13	1.98	78.02	25.98
	88.34	100	1028.67	334.99	3.07	2.13	1.98	78.02	25.98
	88.34	200	1200.92	453.06	2.65	2.13	1.98	78.02	25.98
	84.68	50	882.54	252.78	3.49	2.13	1.93	78.07	25.98
	84.68	100	992.82	334.99	2.96	2.13	1.93	78.07	25.98
	84.68	200	1214.31	453.06	2.84	2.13	1.93	78.07	25.98

Table 13. Results and values adopted for the parameters of concern. Constant moisture content tests.

Fluid	*Sr* (%)	σ'$_3$ (kPa)	q_{ff} (kPa)	q_{fw} (kPa)	q_{ff}/q_{fw}	ε_{rliq}	ε_{rf}	ε_{rw} - ε_{rf}	T_{sf} (10^{-3} N/m)
Water	13.76	50	1160.45	252.78	4.59	80.00	4.38	75.62	70.75
	13.76	100	1348.66	334.99	4.03	80.00	4.38	75.62	70.75
	13.76	200	1701.44	453.06	3.76	80.00	4.38	75.62	70.75
	13.76	400	2071.42	665.36	3.11	80.00	4.38	75.62	70.75
	27.71	50	1148.97	252.78	4.55	80.00	10.25	69.75	70.75
	27.71	100	1430.24	334.99	4.27	80.00	10.25	69.75	70.75
	27.71	200	1700.85	453.06	3.75	80.00	10.25	69.75	70.75
	27.71	400	1872.42	665.36	2.81	80.00	10.25	69.75	70.75
	41.85	50	1303.61	252.78	5.16	80.00	18.70	61.30	70.75
	41.85	100	1561.52	334.99	4.66	80.00	18.70	61.30	70.75
	41.85	200	1779.64	453.06	3.93	80.00	18.70	61.30	70.75
	41.85	400	1850.89	665.36	2.78	80.00	18.70	61.30	70.75
	54.38	100	1596.87	334.99	4.77	80.00	28.30	51.70	70.75
	54.38	200	1822.47	453.06	4.02	80.00	28.30	51.70	70.75
	54.38	400	1842.35	665.36	2.77	80.00	28.30	51.70	70.75
	66.23	100	1699.06	334.99	5.07	80.00	39.21	40.79	70.75
	66.23	200	1760.00	453.06	3.88	80.00	39.21	40.79	70.75
	66.23	400	1996.85	665.36	3.00	80.00	39.21	40.79	70.75
	81.33	100	1682.78	334.99	5.02	80.00	55.67	24.33	70.75
	81.33	200	1708.47	453.06	3.77	80.00	55.67	24.33	70.75
	81.33	400	1735.06	665.36	2.61	80.00	55.67	24.33	70.75
	87.23	50	466.07	107.25	4.35	80.00	62.88	17.12	70.75
	87.23	100	493.51	144.92	3.41	80.00	62.88	17.12	70.75
	87.23	200	618.72	247.44	2.50	80.00	62.88	17.12	70.75
	87.23	400	629.94	382.02	1.65	80.00	62.88	17.12	70.75
	94.37	50	293.37	107.25	2.74	80.00	72.20	7.80	70.75
	94.37	100	349.78	144.92	2.41	80.00	72.20	7.80	70.75
	94.37	200	324.96	247.44	1.31	80.00	72.20	7.80	70.75
	94.37	400	379.31	382.02	0.99	80.00	72.20	7.80	70.75

relative dielectric constant of water and T_{sf} is the superficial tension at the liquid/air interface.

An attempt to build an empirical model for the experimental results presented in Tables 11 to 13 was performed. Several parameters were tested as dependent and independent variables using linear and nonlinear functions to reach the higher R^2 value. Better fitted results were obtained using the ratio q_{ff}/q_{fw} as dependent variable. $(\varepsilon_{rw} - \varepsilon_{rf}).(\sigma_{atm}/\sigma'_3).(T_{sf}/T_{sw})$ and $(\varepsilon_{rw} - \varepsilon_{rf}).(\sigma_{atm}/\sigma'_3)$ were used as independent variables. The ratio (T_{sf}/T_{sw}) was introduced in the modeling because the superficial tension interferes in the capillary suction and therefore in the suction values, mainly at low suction levels.

Equation 5 presents the model used for the prediction of the ratio q_f/q_w as a function of the variables cited above.

$$\frac{q_{ff}}{q_{fw}} = \left\{ \frac{(\varepsilon_{rw} - \varepsilon_{rf})\left(\frac{\sigma_{atm}}{\sigma'_3}\right)\left(\frac{T_{sf}}{T_{sw}}\right) + a}{a + b(\varepsilon_{rw} - \varepsilon_{rf})\left(\frac{\sigma_{atm}}{\sigma'_3}\right)} \right\} \quad (5)$$

where q_{ff} is the deviator stress for samples moistened with the fluid of concern (kPa), q_{fw} is the deviator stress for samples saturated with water (kPa), ε_{rw} is the water relative dielectric constant (~80), ε_{rf} is the relative dielectric constant of the interstitial fluid calculated using Equation 4, σ_{atm} is the atmospheric pressure (~100 kPa), σ'_3 is the effective or net confining stress, T_{sf} is the superficial tension of the fluid of concern (see Table 1), T_{sw} is the water superficial tension, a and b are fitting constants.

Figure 10 presents the fitting of the experimental results presented in Figure 9 with the use of Equation 5. The best fitting parameters were a = 3.7 and b = 0.16, with a value of R^2 = 0.88. Experimental results could also be fitted using the suction values instead of $(\varepsilon_{rw} - \varepsilon_{rf})$. However, the SLRC for the case of ethanol presented several experimental challenges (mainly due to its high vapor pressure) which could not be overcome until now.

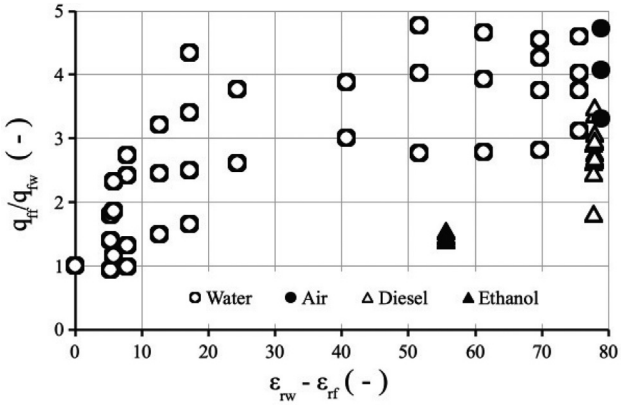

Figure 9. Normalized experimental results.

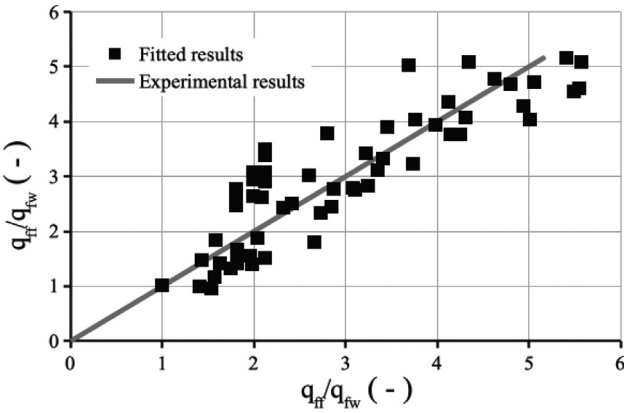

Figure 10. Fitting of experimental results using Equation 5.

5. Conclusions

This paper presents the results of several triaxial tests performed on saturated and unsaturated compacted soil samples filled with different interstitial fluids. A nonlinear relationship was obtained between the shear strength of the soil and the relative dielectric constant of the interstitial fluid, ε_{rf}, so that the higher the ε_{rf}, the lower the shear strength of the soil. The explanation for such behavior is due to the fact that the polarity of the fluid affects the electric fields around the clay particles, the thickness of the double layer and thus the electrical interactions between the particles, which are increased.

An empirical model to predict soil shear strength was proposed, based on the dielectric constant of the interstitial fluid, which presented a good adherence between experimental and fitted results. The use of this model could be an option in more complex scenarios involving multi-phase problems where suction determination/estimation may not be as prompt as the dielectric constant of the interstitial fluid.

References

Almeida, M.S.S. (2016). *Estudo da resistência ao cisalhamento de um solo não saturado quando percolado por fluidos de diferentes constantes dielétricas* [Doctoral thesis, Federal University of Bahia]. Federal University of Bahia's repository (in Portuguese). http://repositorio.ufba.br/ri/handle/ri/28861

Anandarajah, A., & Zhao, D. (2000). Triaxial Behavior of Kaolinite in Different Pore Fluids. *Journal of Geotechnical and Geoenvironmental Engineering*, 126(2), 148-156. https://doi.org/10.1061/(ASCE)1090-0241(2000)126:2(148)

ASTM D971-12. (2012). Standard Test Method for Interfacial Tension of Oil against Water by the Ring Method. *ASTM International, West Conshohocken, PA.*

ASTM D4016-14. (2014). Standard Test Method for Viscosity and Gel Time of Chemical Grouts by Rotational Viscometer (Laboratory Method). *ASTM International, West Conshohocken, PA*. https://doi.org/10.1520/D4016-14

ASTM D5298. (1994). Standard Test Method for Measurement of Soil Potential (Suction) Using Filter Paper. *ASTM International, West Conshohocken, PA*.

ASTM D6438-02. (2008). Standard Test Methods for Determination of the Soil Water Chararcteristic Curve for Desorption Using a Hanging Column, Pressure Extractor, Chilled Mirror Hygrometer, and/or Centrifuge. *ASTM International, West Conshohocken, PA*.

Brown, K.W., & Anderson, D.C. (1983). *Effect of organic solvents on the permeability of clay soils*. US Environmental Protection Agency, Municipal Environmental Research Laboratory.

Brown, K.W., & Thomas, J.C. (1984). Conductivity of three commercially available clays to petroleum products and organic solvents. *Journal of Hazardous Wastes*, 1(4), 545-553. https://doi.org/10.1089/hzw.1984.1.545

Brown, K.W., Thomas, J.C., & Green, J.W. (1986). Field cell verifications of effects of concentrated organic solvents on the conductivity of compacted soils. *Journal of Hazardous Wastes*, 3(1), 1-19. https://doi.org/10.1089/hwm.1986.3.1

Brunnauer, S., Emmett, P.H., & Teller, E. (1938). Adsorption of Gases in Multimolecular Layers. *Journal of the American Chemical Society*, 60(2), 309-319. https://doi.org/10.1021/ja01269a023

Budhu, M., Giese Jr., R.F., Campbell G., & Baumgrass, L. (1991). The permeability of soils with organic fluids. *Canadian Geotechnical Journal*, 28(1), 140-147. https://doi.org/10.1139/t91-015

Calvello, M., Lasco, M., Vassalo, R., & Di Maio, C. (2005). Compressibility and residual shear strength of smectitic clays: influence of pore aqueoussolutions and organic solvents. *Italian Geotechnical Journal*, 1(2005), 34-46.

Davis J.L., & Annan A.P. (1989). Ground penetrating radar for high resolution mapping of soil and rock stratigraphy. *Geophysical Prospecting*, 37(5), 531-551. https://doi.org/10.1111/j.1365-2478.1989.tb02221.x

Di Maio, C., Santoli, L., & Schiavone, P. (2004). Volume change behavior of clays: the influence of mineral composition, pore fluid composition and stress state. *Mechanics of Materials*, 36(5-6), 435-451. https://doi.org/10.1016/S0167-6636(03)00070-X

Fang, H.Y. (1997). *Introduction to Environmental Geotechnology*. CRC Press.

Fernandez, F., & Quigley, R. (1985). Hydraulic conductivity of natural clays permeated with simple liquid hydrocarbons. *Canadian Geotechnical Journal*, 22(2), 205-214. https://doi.org/10.1139/t85-028

Fredlund, D.G., & Xing, A. (1994). Equations for the soil-water characteristic curve. *Canadian Geotechnical Journal*, 31(4), 521-532. https://doi.org/10.1139/t94-061

Garcia, J.R., Rodrigues, R.A., & Lollo, J.A. (2004). A influência de diferentes fluidos de inundação no colapso estrutural de um solo arenoso laterítico. *Civil Engineering Journal*, 21, 49-58 (in Portuguese).

Gouy, G. (1910). Sur la constitution de la charge electrique a la surface d'un electrolyte. *Anniue Physique*, 4(9), 457-468 (in French). https://doi.org/10.1051/jphystap:019100090045700

Halliday, D., Resnick, R., & Walker, J. (2007). *Fundamentos de Física: Eletromagnetismo*. LTC (in Portuguese).

Hillel, D. (1980). *Fundamentals of Soil Physics*. Academic Press.

Helmholtz, H.V. (1879). Studien über electrische Grenzschichten. *Annalen der Physik*, 243(7), 337-382 (in German). https://doi.org/10.1002/andp.18792430702

Li, J., Smith, J.A., & Winquist, A. (1996). Permeability of earthen liners containing organobentonite to water and two organic liquids. *American Chemical Society*, 30(10), 3089-3093. https://doi.org/10.1021/es960172p

Kaya, A., & Fang, H. (2005). Experimental evidence of reduction in attractive and repulsive forces between clay particles permeated with organic liquids. *Canadian Geotechnical Journal*, 42(2), 632-640. https://doi.org/10.1139/t04-099

Oliveira, J.C.S. (2001). *Contaminação de sedimentos argilosos por combustíveis automotivos: problemas de avaliação da permeabilidade* [Unpublished doctoral thesis]. Federal University of Bahia (in Portuguese).

Schramm, M., Warrick, A.W., & Fuller, W.H. (1986). Permeability of soils to four organic liquids and water. *Hazardous Waste and Hazardous Materials*, 3(1), 21-27. https://doi.org/10.1089/hwm.1986.3.21